THE BELL SYSTEM TECHNICAL JOURNAL
Vol. 60, No. 10, December 1981
Printed in U.S.A.

Study of a Time-Compression Technique for TV Transmission Using a Chirp Filter and Envelope Detection

By K. Y. ENG and B. G. HASKELL

(Manuscript received January 19, 1981)

We study a time-compression (or expansion) technique for possible application in communication signal processing, e.g., broadcast-quality TV transmission through satellites. The method uses a linear chirp, a linear dispersive filter realized by surface acoustic wave devices and an envelope detector. This technique is heuristic and can be viewed as a quasistationary model of the FM wave involved. Numerical results show that excessive distortion is created, and its application to TV transmission is not suitable unless some kind of equalization is provided. One such form of equalization is the chirp transform processor which involves considerably more complexity. Simpler equalizations may be possible but do not seem to be straightforward.

I. INTRODUCTION

We study a time-compression technique motivated by the long-standing interest in transmitting multiple broadcast-quality color TV signals through a single satellite transponder, i.e., a usable RF bandwidth of 36 MHz in a communications satellite such as COMSTAR. This can be done by the use of frequency division multiplexing (FDM). However, the nonlinearity of the transponder can cause serious intelligible crosstalk and intermodulation interference between the FM carriers unless the satellite power amplifier is backed off substantially. Such a backoff, in turn, leads to a reduction in the downlink carrier-to-noise ratio. As a result, there exists an optimum trade-off between the crosstalk and s/n's, which limits the overall system performance, and achieving broadcast-quality TV transmission becomes difficult.

It is possible to time compress each scan line of a color TV signal by

the use of a linear chirp, a linear dispersive filter (LDF) and an envelope detector. Two or more time-compressed scan lines from different, but synchronized, TV signals can then be time multiplexed together in the time duration of an ordinary TV scan line. This concept of time-compression multiplexing (TCM) is not new,[1,2] but recent advances in fast analog-to-digital converters, digital-to-analog converters and charge-coupled devices have greatly facilitated the implementation of time compression or expansion. However, because of their present limitations on bandwidth and speed, time-compression factors for achievable TV signals are only 2 or 3. For large time compressions, LDFs realizable by surface acoustic wave (SAW) technology are promising candidates because of their large time-bandwidth property. In addition to high speed, the TV application also requires extremely high signal fidelity. There are other applications on the high-speed time expansion (or compression) of waveforms where the distortion requirement is less stringent than the TV transmission case. In the specific case of multiple TV transmissions through a single satellite transponder, there are many advantages in using TCM, e.g., higher transponder efficiency, no intermodulation, no crosstalk, possible compatibility with time division multiplex (TDM) operations, etc. The crucial question is, of course, how much distortion the compression/expansion process would introduce on the signals. This paper gives both analysis and numerical examples that illustrate the method.

The study revealed that considerable distortion is introduced by these operations, and its application to broadcast-quality TV transmission would require SAW filter performance beyond the present state of the art. However, if the distortion requirement can be relaxed somewhat, then the present approach is advantageous because of its simplicity. On the other hand, if high signal fidelity is required, then some kind of equalization is needed for the present technique. This has motivated the study of an extension of the present method which is capable of producing high signal quality with SAW filter requirements within the present state of the art even at compression factors of 10 or more, but at the expense of higher complexity. This latter development is not discussed here but is covered in Ref. 3. The remainder of the paper covers the theoretical analysis and computer simulation. However, the discussion of either subject by itself is not adequate for the complete understanding of the system. The theoretical analysis establishes that although the basic concept was derived heuristically through physical interpretations, it can be viewed as a quasi-stationary approximation to the time-compression process. The computer simulation, on the other hand, provides the quantitative results that lead to the conclusion that the resulting distortion is excessive for today's SAW filter parameters.

II. THEORETICAL ANALYSIS

In this section, we describe and analyze the proposed compression method using TV as an example. We first describe a heuristic argument of how the technique is supposed to work. We then derive the impulse response of a general LDF—the understanding of which is important to the subsequent analysis and simulation. A brief step-by-step analysis of the compression process is shown, and its result reveals that the technique can be interpreted as a quasi-stationary approximation of the chirp signal. The mathematical expressions describing the time compressor are complicated; thus, numerical results are obtained using a computer simulation discussed in Section III. Various other properties are also discussed.

2.1 A physical interpretation

A block diagram is shown in Fig. 1. The input signal $v(t)$ consists of successive scan lines, each with a duration of T_l seconds, and the voltage is biased to be positive. It is multiplied synchronously by a periodic chirp signal $c(t)$ with a center frequency f_0 and a chirp range of Δf_c. The instantaneous frequency of $c(t)$ sweeps linearly from $(f_0 - \Delta f_c/2)$ to $(f_0 + \Delta f_c/2)$ over each scan line duration T_l. The lowest frequency of the chirp signal is assumed to be much greater than the highest frequency in the TV signal. The input $x(t)$ to the LDF is then an amplitude-modulated chirp waveform. For simplicity, let us restrict our attention to a single scan line, say $(0, T_l)$. In this interval, $x(t)$ chirps from $(f_0 - \Delta f_c/2)$ to $(f_0 + \Delta f_c/2)$ with the TV signal as the

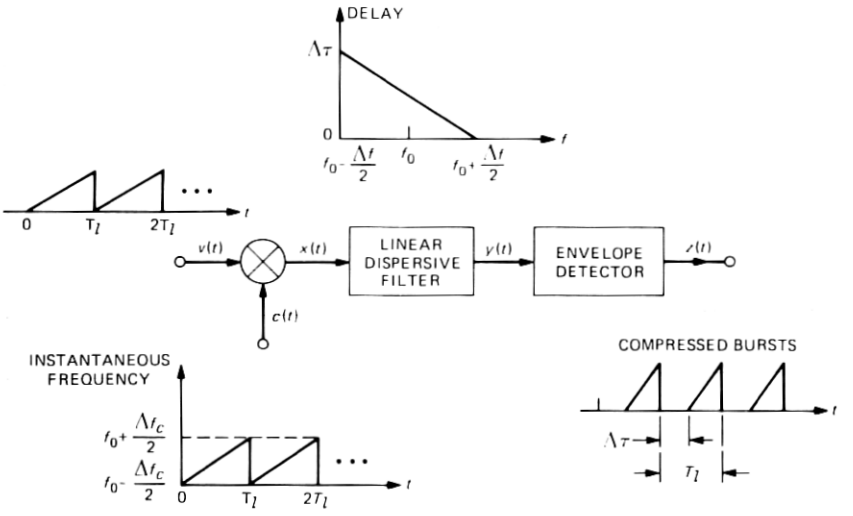

Fig. 1—Time-compression filter.

envelope modulation. As for the LDF, we assume that it has a bandwidth Δf centered at f_0, and $\Delta f \geq \Delta f_c$.

Again, for the purpose of a simple illustration, let us assume that $\Delta f = \Delta f_c$ and, over its passband, the LDF has a constant gain and a linear group delay characteristic decreasing from $\Delta\tau$ to zero, where $\Delta\tau$ is the delay dispersion of the LDF. At the time instant $t = 0$, $x(t)$ has an instantaneous frequency $(f_0 - \Delta f_c/2)$ and an envelope magnitude proportional to $v(0)$. This "envelope piece" is delayed by $\Delta\tau$ as it transits through the LDF. Similarly, at $t = T_l$, the instantaneous frequency of $x(t)$ is the highest chirp frequency which gives a zero delay for the passage through the LDF. In between these two end points, the envelope of $x(t)$ is delayed linearly from $\Delta\tau$ to zero. Equivalently, the envelope of $x(t)$ over the interval $(0, T_l)$ is time compressed into $(\Delta\tau, T_l)$ in the LDF output. An envelope detector is then used to retrieve the time-compressed TV signal. Similar compression occurs for all the other scan lines, and as a result, the envelope detector output consists of a sequence of compressed TV bursts. If we denote the duration of each burst by T_c, the ratio (T_l/T_c) is called the time-compression ratio (TCR).

It is easy to show that, in general, for a given set of T_l, $\Delta\tau$, Δf, and Δf_c,

$$T_c = T_l - \frac{\Delta\tau}{\Delta f}\Delta f_c, \tag{1}$$

where $0 \leq T_c \leq T_l$, $\Delta f_c \leq \Delta f$, and the compression ratio is

$$\text{TCR} = \left(1 - \frac{\Delta\tau}{\Delta f}\frac{\Delta f_c}{T_l}\right)^{-1}. \tag{2}$$

It is clear from the above description that time expansion is also possible by the use of an increasing delay characteristic in the LDF, and in such a case, the filter will become a time-expansion filter.

2.2 Impulse response of a general LDF

We consider the general case of an idealized LDF as shown in Fig. 2a. The bandwidth of the filter is Δf centered at f_0. The group delay varies linearly over the passband as shown in the diagram. The transfer function of the filter, using analytic-signal notation, is

$$H(f) = \begin{cases} \exp\left\{-j2\pi\left[(f - f_0)\tau_0 + \dfrac{(f - f_0)^2}{2\alpha} + \phi_1\right]\right\}, \\ \qquad -\dfrac{\Delta f}{2} \leq f - f_0 \leq \dfrac{\Delta f}{2}, \\ 0, \qquad \text{elsewhere}, \end{cases} \tag{3}$$

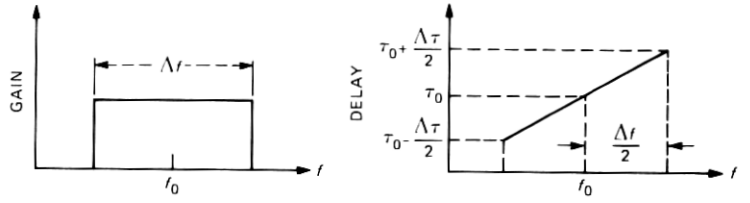

(a)

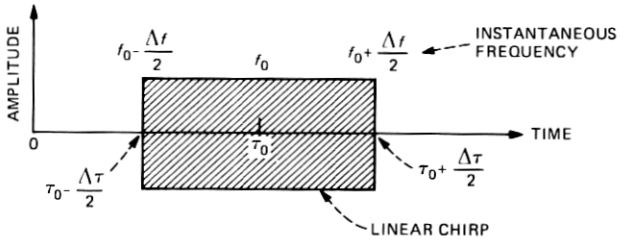

(b)

Fig. 2—Characteristics and impulse response of an LDF. (a) Transfer function. (b) Impulse response.

where

$$\alpha \triangleq \frac{\Delta f}{\Delta \tau}, \tag{4}$$

τ_0 is the group delay at f_0, and ϕ_1 is a constant. The inverse Fourier transform of $H(f)$ gives the impulse response $h(t)$. The derivation for $h(t)$ is given in Appendix A. Neglecting some small envelope and phase perturbations, a good approximation (sufficient for our present consideration) for $h(t)$ is

$$h(t) = \begin{cases} \cos 2\pi\left[\left(f_0 - \dfrac{\Delta f}{2}\right)t + \dfrac{\alpha}{2}t^2 + \phi_2\right], \\ \qquad \tau_0 - \dfrac{\Delta\tau}{2} \le t \le \tau_0 + \dfrac{\Delta\tau}{2}, \\ 0, \qquad \text{elsewhere}, \end{cases} \tag{5}$$

where the multiplying constant has purposely been dropped, and ϕ_2 is a constant. A sketch of $h(t)$ is shown in Fig. 2b. It is a linear chirp waveform starting at $\tau_0 - \Delta\tau/2$ and ending at $\tau_0 + \Delta\tau/2$, with the instantaneous frequency varying from $f_0 - \Delta f/2$ to $f_0 + \Delta f/2$ at a chirp rate of α.

2.3 Analysis of time compression

In this analysis, we again restrict our discussion to a single scan line

for simplicity. We denote this input scan line by $A(t)$ in the interval $(0, T_l)$. Referring to Fig. 1, the linear chirp signal is given by

$$c(t) = \cos 2\pi\left[\left(f_0 - \frac{\Delta f_c}{2}\right)t + \frac{\beta}{2}t^2 + \phi_3\right], \qquad 0 \le t \le T_l, \tag{6}$$

where β is the chirp rate defined by

$$\beta = \frac{\Delta f_c}{T_l}, \tag{7}$$

and ϕ_3 is a constant. The parameters f_0 and Δf_c are the chirp center frequency and deviation, respectively. There are also two implicit assumptions: (*i*) $f_0 \gg \Delta f_c$; and (*ii*) $f_0 \gg$ the highest frequency in the TV signal.

The LDF input is the product of the TV input $A(t)$ and $c(t)$, i.e.,

$$x(t) = A(t)\cos 2\pi\left[\left(f_0 - \frac{\Delta f_c}{2}\right)t + \frac{\beta}{2}t^2 + \phi_3\right], \qquad 0 \le t \le T_l. \tag{8}$$

To obtain the LDF output, we can either use the time-domain approach by convolving $x(t)$ with the impulse response $h(t)$ of the LDF, or use frequency domain analysis by multiplying the Fourier transform of $x(t)$ by the LDF transfer function and then performing an inverse transform. The former method is much simpler and is presented here. The latter is tedious, offers no additional insight, and is, therefore, deleted for brevity.

The LDF is assumed to have an extended passband over $(f_0 - \Delta f/2, f_0 + \Delta f/2)$, where $\Delta f > \Delta f_c$. Its delay characteristic is shown in Fig. 3. Note that the delay slope is given by

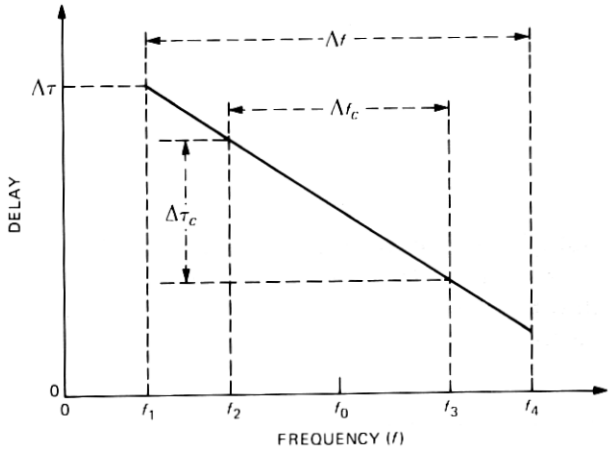

Fig. 3—Delay characteristic of the LDF.

$$\alpha^{-1} = \frac{\Delta\tau}{\Delta f}. \tag{9}$$

Also note in Fig. 3 that the delay at $f_0 + \Delta\tau/2$ is zero, as some constant delay through the device has been dropped for simplicity. Using the result of Section 2.2, the impulse response of the LDF is

$$h(t) = \begin{cases} \cos 2\pi\left[f_1 t - \frac{\alpha}{2} t^2 + \phi_4 \right], & 0 \le t \le \Delta\tau, \\ 0, & \text{elsewhere}, \end{cases} \tag{10}$$

where $f_1 \triangleq f_0 - \Delta f/2$, and ϕ_4 is a constant. The LDF output is then

$$\begin{aligned} y(t) &= \int_{-\infty}^{\infty} x(\tau) h(t-\tau)\, d\tau \\ &= \int_{T_1}^{T_2} \frac{A(\tau)}{2} \\ &\quad \times \left\{ \cos 2\pi\left[\Phi(t) + (\alpha t - \Delta f_c - f_4 + f_3)\tau + (\beta - \alpha)\frac{\tau^2}{2} \right] + \right. \\ &\quad \left. \cos 2\pi\left[\Phi(t) + (2f_0 - \alpha t + f_4 - f_3)\tau + (\beta + \alpha)\frac{\tau^2}{2} \right] \right\} d\tau, \\ &\quad 0 \le t \le T_l + \Delta\tau, \end{aligned} \tag{11}$$

where the limits of integration are defined by

$$T_1 \triangleq \max(0,\ t - \Delta\tau), \tag{12}$$

$$T_2 \triangleq \min(t,\ T_l), \tag{13}$$

f_3 and f_4 are defined in Fig. 3, and

$$\Phi(t) \triangleq f_4 t - \frac{\alpha}{2} t^2 + \phi_4 . \tag{14}$$

A constant phase term has been dropped in (eq. 11), and we will neglect all unimportant constant multipliers and phase shifts in subsequent discussions. The integral of the second cosine term in eq. (11) can be discarded because of the high frequency component $2f_0\tau$ in the integrand. Therefore, $y(t)$ becomes

$$\begin{aligned} y(t) = \int_{T_1}^{T_2} A(\tau) \cos 2\pi\Big[& \Phi(t) + (\alpha t - \Delta f_c - f_4 + f_3)\tau \\ & + (\beta - \alpha)\frac{\tau^2}{2} \Big] d\tau, \qquad 0 \le t \le T_l + \Delta\tau. \end{aligned} \tag{15}$$

Let us examine the above integral expression carefully. Using analytic-signal notation, we rewrite it as

$$y(t) = \int_{T_1}^{T_2} A(\tau) \exp\left\{ j2\pi \left[\Phi(t) + (\alpha t - \Delta f_c - f_4 + f_3)\tau + (\beta - \alpha)\frac{\tau^2}{2} \right] d\tau \right\}$$

$$= \exp j2\pi\Phi(t) \int_{T_1}^{T_2} A(\tau) \exp\left\{ j2\pi \left[(\alpha t - \Delta f_c - f_4 + f_3)\tau + (\beta - \alpha)\frac{\tau^2}{2} \right] d\tau \right\},$$

$$0 \le t \le T_l + \Delta\tau. \tag{16}$$

In this form, we can define a complex envelop for $y(t)$ as

$$A_y(t) \triangleq \int_{T_1}^{T_2} A(\tau) \exp\left\{ j2\pi \left[(\alpha t - \Delta f_c - f_4 + f_3)\tau + (\beta - \alpha)\frac{\tau^2}{2} \right] d\tau \right\}, \qquad 0 \le t \le T_l + \Delta\tau. \tag{17}$$

In the above, note that $A(\tau)$ is a slow-moving function while the exponential term contains a highly oscillatory chirp given by the derivative of the bracketed argument with respect to τ, i.e.,

$$f_i(\tau) = (\alpha t - \Delta f_c - f_4 + f_3) + (\beta - \alpha)\tau, \qquad T_1 \le \tau \le T_2. \tag{18}$$

This can also be obtained by simply taking the difference of the instantaneous frequencies of $x(\tau)$ and $h(t - \tau)$ in eq. (11). The convolution integral involved is illustrated in Fig. 4, where we show $x(\tau)$ and also the corresponding $f_i(\tau)$ at a fixed $t = t_1$. It can be seen that $A_y(t_1)$ is given by an integral over (T_1, T_2) of a linear chirp waveform at a chirp rate of $(\beta - \alpha)$ and with an envelope modulation $A(\tau)$. Furthermore, the chirp frequency f_i inside (T_1, T_2) may vanish at some τ as shown in Fig. 4. In such a case, the value of $y(t_1)$ is dominated by the integral eq. (15) over the small interval surrounding that τ, where f_i goes to zero. This is, of course, the well-known quasi-stationary approximation. The approximation is good if the chirp rate $(\beta - \alpha)$ and the interval (T_1, T_2) are large, and $A(\tau)$ variation is slow by comparison. Using this approximation, at $t = t_1$ inside the valid interval $(0, T_l + \Delta\tau)$,

$$A_y(t_1) \approx kA(\tau_1), \tag{19}$$

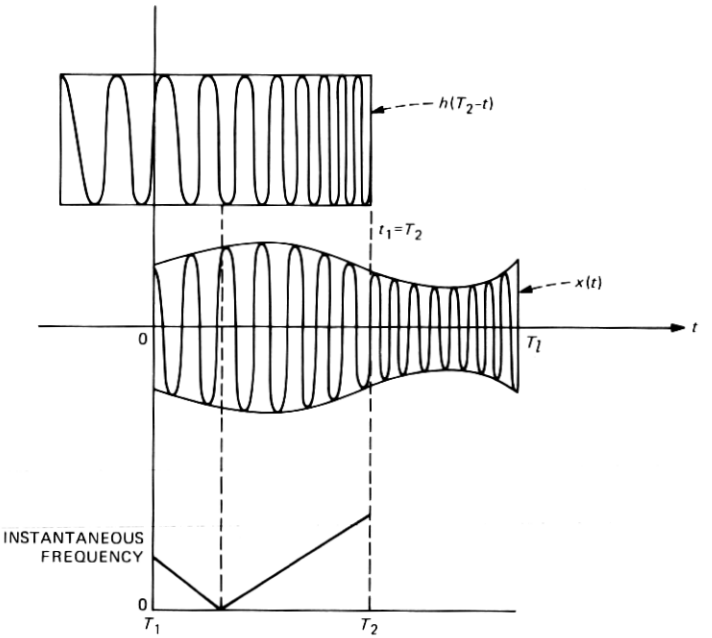

Fig. 4—Convolution integral.

where k is a constant, and τ_1 is obtained by solving eq. (18) with f_i set to zero and $t = t_1$, i.e.,

$$\tau_1 = \frac{\alpha t_1 - \Delta f_c - f_4 + f_3}{\beta - \alpha}. \tag{20}$$

This quasi-stationary approximation is indeed equivalent to the physical interpretation described in Section 2.1. As a check, let us derive the TCR from the approximation above. We know that $A(\tau_1)$ is nonzero only if $0 \leq \tau_1 \leq T_l$. The corresponding t_1 can be solved for using eq. (20), and the end points of t_1 constitute the interval T_c, i.e.,

$$T_c = \frac{(\Delta f_c + f_4 - f_3) - T_l(\beta - \alpha)}{\alpha} - \frac{(\Delta f_c + f_4 - f_3)}{\alpha}$$

$$= T_l\left(1 - \frac{\beta}{\alpha}\right). \tag{21}$$

Therefore,

$$\text{TCR} = \left(1 - \frac{\beta}{\alpha}\right)^{-1}, \qquad \alpha \geq \beta, \tag{22}$$

which agrees with eq. (2) with the substitutions of α and β according

to the definition eqs. (4) and (7), respectively. See Section 2.4 for a continued discussion of $A_y(t)$.

To finish our analysis of the time compression, we return to $y(t)$ in eq. (15) and expand the cosine term:

$$y(t) = y_c(t)\cos 2\pi\Phi(t) - y_s(t)\sin 2\pi\Phi(t), \tag{23}$$

where

$$y_c(t) \triangleq \int_{T_1}^{T_2} A(\tau)\cos 2\pi\left[(\alpha t - \Delta f_c - f_4 + f_3)\tau + (\beta - \alpha)\frac{\tau^2}{2}\right]d\tau \tag{24}$$

and

$$y_s(t) \triangleq \int_{T_1}^{T_2} A(\tau)\sin 2\pi\left[(\alpha t - \Delta f_c - f_4 + f_3)\tau + (\beta - \alpha)\frac{\tau^2}{2}\right]d\tau. \tag{25}$$

In eq. 25, $y_c(t)$ and $y_s(t)$ can be viewed as the in-phase and quadrature components of $y(t)$ after synchronous demodulation. The envelope detector output is then

$$z(t) = [y_c^2(t) + y_s^2(t)]^{1/2}. \tag{26}$$

2.4 Some fundamental properties

We have just derived mathematical expressions for the time-compression process. These expressions are too complicated for easy interpretation. However, we have demonstrated that the technique works if a quasi-stationary approximation is made for the chirp waveform. In other words, the instantaneous frequency of the chirp wave could be used as if it were a stationary carrier frequency in a steady state analysis.

Making such an assumption, it is seen from eq. (2) that infinite compression, TCR = ∞, results if $\Delta f = \Delta f_c$ and $\Delta\tau = T_l$ ($\alpha = \beta$). But from eqs. (15), (24), and (25), it is obvious that the LDF output after synchronous detection (for $\alpha = \beta$) will actually become the Fourier transform of the input envelope $A(t)$. This can also be recognized as the well-known chirp transform or real-time transform[4,5] commonly used in chirp radar and SAW processors. Therefore, the quasi-stationary model is invalid for this case.

A case where the quasi-stationary approximation clearly holds is where $\Delta f_c \to \infty$ and $\alpha^{-1} \to 0$, i.e., the chirp range is very large, and the delay slope of the LDF is close to zero. The result is, of course, a very slight compression, i.e., the TCR is slightly larger than 1. Therefore, without doing any specific calculation, we see that the quasi-stationary assumption is valid, at best, for small TCRs, and it breaks down somewhere between TCR = 1 and ∞. Since our practical applications

require TCR ≥ 2, the case of TCR $= 2$ becomes most interesting and is investigated in the simulation later.

Let us now assume the quasi-stationary model and see what kind of distortion would result. The input to the LDF can be expressed as a multitone AM signal:

$$\tilde{x}(t) = \left(1 + \sum_{j=1}^{N} m_j \cos\omega_j t\right)\cos\omega_c t, \tag{27}$$

where ω_j are the angular modulating frequencies, and ω_c is the angular carrier frequency at some fixed instant of time. Let τ_c be the delay of the LDF at $\omega = \omega_c$. The phase characteristic of the LDF is

$$\phi(\omega) = -(\tau_c + \omega_c/\alpha)\omega + \omega^2/(2\alpha) + c, \tag{28}$$

where c is a constant, and α is defined in eq. (9). The LDF output is

$$\begin{aligned}\tilde{y}(t) = {} & \cos\left[\omega_c t + (\tau_c + \omega_c/\alpha)(-\omega_c) + \frac{\omega_c^2}{2\alpha} + c\right] \\ & + \sum_{j=1}^{N} \frac{m_j}{2}\left\{\cos\left[\omega_c t + \omega_j t - \left(\tau_c + \frac{\omega_c}{\alpha}\right)(\omega_c + \omega_j) + \frac{(\omega_c + \omega_j)^2}{2\alpha} + c\right]\right. \\ & \left. + \cos\left[\omega_c t - \omega_j t - \left(\tau_c + \frac{\omega_c}{\alpha}\right)(\omega_c - \omega_j) + \frac{(\omega_c - \omega_j)^2}{2\alpha} + c\right]\right\}. \end{aligned} \tag{29}$$

In the above expression, various sidebands of the input AM signal are delayed asymmetrically about the carrier frequency. This would, of course, distort the signal. After some tedious manipulations, the envelope of $\tilde{y}(t)$ is found to be

$$\begin{aligned}\tilde{Y}(t) = \Bigg\{ & \left[1 + \sum_{j=1}^{N} m_j \cos\omega_j(t - \tau_c)\cos\left(\frac{\omega_j^2}{2\alpha}\right)\right]^2 + \\ & \left[\sum_{j=1}^{N} m_j \cos\omega_j(t - \tau_c)\sin\left(\frac{\omega_j^2}{2\alpha}\right)\right]^2\Bigg\}^{1/2}. \end{aligned} \tag{30}$$

Comparing $\tilde{Y}(t)$ and $\tilde{x}(t)$, it is obvious that distortionless transmission results only if $\omega_j^2/(2\alpha) \ll 1$. More importantly, the distortion in $\tilde{Y}(t)$ is dependent on the input signal and, therefore, cannot be equalized easily. On the other hand, if synchronous demodulation is used in place of envelope detection, we obtain the first square bracket term in eq. (30), i.e.,

$$\tilde{Y}_s(t) = 1 + \sum_{j=1}^{N} m_j \cos\omega_j\,(t - \tau_c)\cos\left(\frac{\omega_j^2}{2\alpha}\right), \tag{31}$$

where the distortion shows up as $\cos[\omega_j^2/(2\alpha)]$ which is independent of the input signal, and equalization is thereby feasible. To do synchro-

nous demodulation, we need to know the instantaneous frequency of the carrier in $y(t)$, the LDF output, which we have not addressed so far. Let us do so in the following.

Stating eq. (16) again,

$$y(t) = \exp[j2\pi\Phi(t)] \int_{T_1}^{T_2} A(\tau) \exp\left[j(\beta - \alpha) \frac{\tau^2}{2} \right] \cdot \exp[j2\pi(\alpha t - \Delta f_c - f_4 + f_3)\tau] d\tau. \quad (32)$$

In the above we have, in part, an output chirp frequency of $d\Phi/dt = (f_4 - \alpha t)$. The integral part, on the other hand, can be interpreted in two different ways: (*i*) It is a "quadratic" chirp transform of $A(\tau)$. As such, little is known about this transform. (*ii*) It is the Fourier transform of $A(\tau) \exp[j2\pi(\beta - \alpha)\tau^2/2]$, where $A(\tau)$ can be viewed as an envelope modulation on a chirp signal with frequency $(\beta - \alpha)\tau$. Equivalently, it is the convolution of the Fourier transform of $A(\tau)$ and that of the chirp signal. The result may very well contain high frequency components depending on the magnitude of $(\beta - \alpha)$ and the shape of $A(\tau)$. In fact, simulation results show that the instantaneous frequency of $y(t)$ can be quite different from $(f_4 - \alpha t)$. Therefore, frequency predictability is difficult in the general case, and synchronous detection as discussed above cannot be used easily.

The following is a summary of the analytic results:

(*i*) The mathematical expressions are complicated, and simulation is necessary to obtain numerical insights.

(*ii*) The compression operation can be justified by a quasi-stationary model. Under this model and with envelope detection, multitone AM leads to nonequalizable distortion. Furthermore, the quasi-stationary model is valid only for small TCRs.

(*iii*) Synchronous detection is very difficult because of frequency unpredictability.

III. SIMULATION

This section describes simulation results. These numerical results show that the proposed technique indeed time compresses the input signal, but the output distortion is probably unacceptable for TV transmission using today's SAW devices.

3.1 Preliminary set-up

A computer subroutine was written to simulate the time-compression operation. It accepts an arbitrary input $A(t)$ defined in the interval $(0, T_l)$ and outputs $y(t)$, $y_c(t)$, and $y_s(t)$, given by eqs. (15), (21), and (22), respectively. Note that $y(t)$ is the RF output of the LDF, and $y_c(t)$ and $y_s(t)$ are the in-phase and quadrature components after synchro-

nous demodulation with $\Phi(t)$ so that the ideal envelope detector output $z(t)$ can be easily calculated from eq. (23). Also note that all three outputs have the same integral form, i.e.,

$$I = \int_{t_1}^{t_2} f(t)\cos[2\pi(at^2 + bt + c)]dt, \tag{33}$$

where we can assume $t_1 \geq 0$, $t_2 \geq t_1$, and $a > 0$. In the computer program, we break the interval $(0, T_l)$ into many small segments such that within each segment, a linear approximation of $A(t)$ is valid. After doing so, the integration over each of these segments can be done in the form of eq. (33) with

$$f(t) \approx mt + k. \tag{34}$$

The limits of integration t_1 and t_2 in eq. (33) are, of course, the end points of the small time segment. Using the linear representation eq. (34) for $f(t)$, I in eq. (33) can be integrated in closed form in terms of Fresnel integrals, and the result is

$$I = mI_2 + kI_1, \tag{35}$$

where

$$I_1 = [\pi/(2p)]^{1/2}\{[C(z_2) - C(z_1)]\cos B - [S(z_2) - S(z_1)]\sin B\}, \tag{36}$$

$$I_2 = \frac{\cos B}{2p}\{\sin x_2^2 - \sin x_1^2 - q[\pi/(2p)]^{1/2}[C(z_2) - C(z_1)]\}$$
$$+ \frac{\sin B}{2p}\{\cos x_2^2 - \cos x_1^2 + q[\pi/(2p)]^{1/2}[S(z_2) - S(z_1)]\}, \tag{37}$$

and

$$p = 2\pi a; \quad q = 2\pi b; \quad r = 2\pi c, \tag{38}$$

$$B = r - \left(\frac{q}{2\sqrt{p}}\right)^2, \tag{39}$$

$$x_1 = \sqrt{p}t_1 + \frac{q}{2\sqrt{p}}, \tag{40}$$

$$x_2 = \sqrt{p}t_2 + \frac{q}{2\sqrt{p}}, \tag{41}$$

$$z_1 = \frac{x_1}{\sqrt{x/2}}, \tag{42}$$

$$z_2 = \frac{x_2}{\sqrt{\pi/2}}. \tag{43}$$

The Fresnel integrals in eq. (36) are defined by

$$C(z) = \int_0^z \cos\left(\frac{\pi}{2}x^2\right) dx \tag{44}$$

and

$$S(z) = \int_0^z \sin\left(\frac{\pi}{2}x^2\right) dx. \tag{45}$$

There are also some simpler cases, e.g., $a = 0$ or $b = 0$, which are not shown for brevity. Since time expansion can be achieved by reversing the delay slope of the LDF, the subroutine for simulating the time compression can also be used to simulate the time-expansion filter. Examples of both time compression and expansion will be shown later.

In all subsequent simulations, the input is always

$$A(t) = \begin{cases} 1, & 0 \le t \le T_l \quad (T_l = 64\ \mu s) \\ 0, & \text{otherwise} \end{cases}. \tag{46}$$

This rectangular pulse is, of course, not a representative of the video signal. However, except for edge "ringings," the system should compress the pulse properly, and peak-to-peak (p-p) ripples at the center portion of the output pulse should give an indication of the magnitude of distortion involved. To examine the outputs $y(t)$, $y_c(t)$, and $y_s(t)$, we have also developed a set of programs to estimate the instantaneous frequency at various time instants of $y(t)$, as well as the p-p ripples of the output pulse.

Because of the complexity of the equations and various computer routines, it is not easy to assure that there is no bug in the programs. However, we did make some runs for the special case $\alpha = \beta$ (Fourier transform case) where results are known. The waveforms $y_c(t)$, $y_s(t)$, and $z(t)$, and the output chirp frequency and offset frequency of the LDF given by eq. (31) were all verified carefully. Such a check assures the validity of the computer programs.

3.2 Examples of time compression

Four examples of time compression are discussed in this section. They all have TCR = 2 (i.e., 2:1 compression) and an input given by eq. (46) (see Fig. 5a). The chirp frequency range Δf_c for the input $x(t)$ to the LDF is (f_2, f_3), while the passband Δf of the LDF extends over (f_1, f_4). The delays at f_i are denoted by τ_i ($i = 1$ to 4), respectively. The delay dispersion of the LDF is defined by $\Delta\tau = \tau_1 - \tau_4$. The descriptions for these examples are as follows:

(i) The key parameters for the LDF are shown in Fig. 5b. In this example, we let $f_1 = f_2$, $f_3 = f_4$ and choose

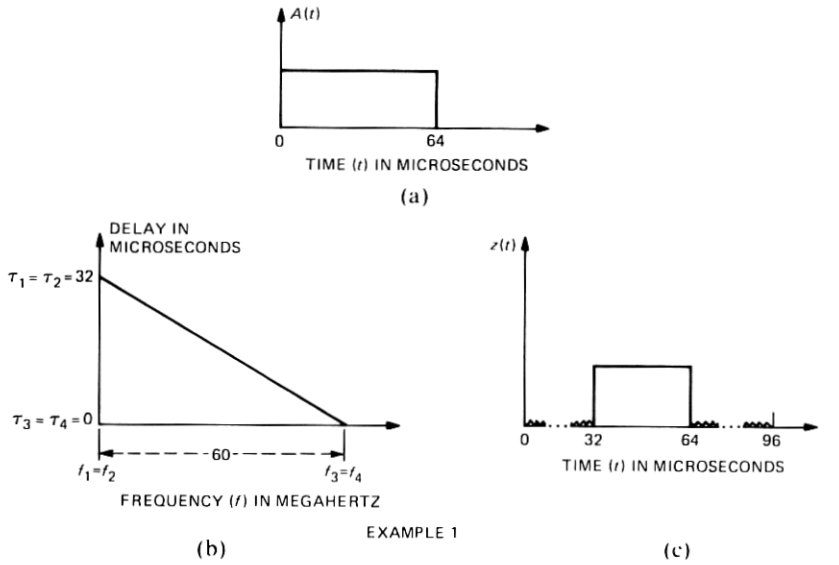

Fig. 5—Parameters for time-compression technique. Example 1—(a) Input pulse (t); (b) Delay of LDF; (c) Expected output (t).

$$\Delta f_c = \Delta f = 60 \text{ MHz}. \tag{47}$$

From eq. (2), TCR = 2 with $\Delta\tau = 32$ μs. The time-bandwidth product (BT) of the LDF is defined by

$$\text{BT} = (\Delta f)(\Delta\tau). \tag{48}$$

Here, BT = 1920. Bandwidth product $\approx$ 10,000 to 50,000 is considered as a practical range for SAW filters. The "expected" output is illustrated in Figure 5c where the output compressed pulse appears between t = 32 μs and 64 μs. The small ripples in the time intervals, 0 to 32 μs and 64 to 96 μs are to illustrate the nonzero output of the LDF in these regions.

(*ii*) The LDF parameters are shown in Fig. 6a and the expected output in Fig. 6b. Here, $\Delta f_c = 60$ MHz which is the same as in Example 1 (Fig. 5), but $\Delta\tau$ and Δf are both increased by a factor of 3. With $\Delta f = 180$ MHz and $\Delta\tau = 96$ μs, BT = 17,280.

(*iii*) The parameters are shown in Fig. 7a, and the expected output is the same as that of Example 2 (Fig. 6) because the delay dispersion has remained the same. We increased Δf to 600 MHz yielding BT = 57,600, which is probably a little beyond present-day state of the art. We used $\Delta f_c = 200$ MHz.

(*iv*) The parameters are shown in Figs. 6a and 6b. This is essentially the same as Example 3 in Fig. 7a, except Δf is increased to 1200 MHz,

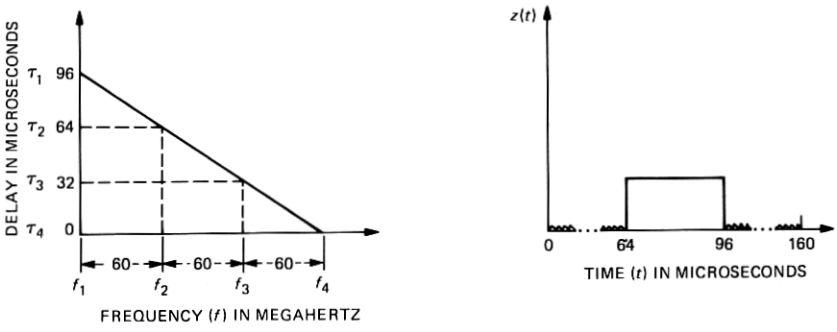

Fig. 6—Parameters for time-compression technique. Example 2—(a) Delay of LDF; (b) Expected output (t).

and BT = 115,200. This is probably not realizable in the near future. We used $\Delta f_c = 400$ MHz.

The above examples are arranged to illustrate the effect of increasing Δf (or the strengthening of the quasi-stationary model).

With the input being a pulse 64-μs long, the expected output for all examples is a compressed pulse, 32 μs in duration (TCR = 2). This is indeed so from the simulation results which show a compressed pulse approximately 32 μs long in the expected time slot. The output outside the compressed pulse duration is at least an order of magnitude lower. However, inside this compressed pulse, there are ripples created by the compression process, and these ripples are the resulting distortion that we are trying to estimate. The ripples are largest at the edges of the compressed pulse and smallest toward the center. Also, the ripples at the center are indications of the "best" performance of the time-compression filter. In our computer routines to estimate distortions,

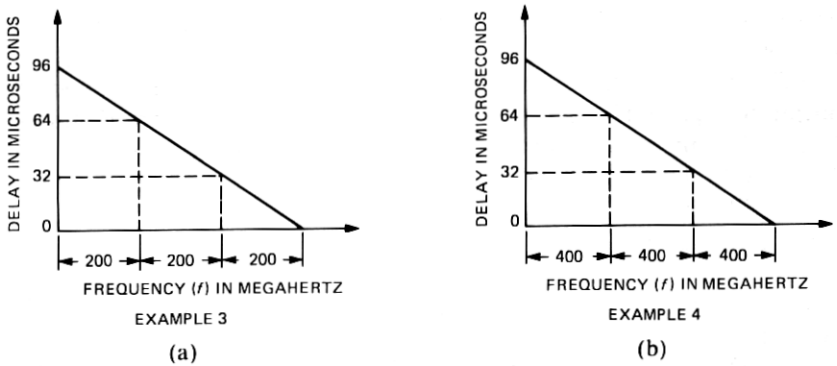

Fig. 7—Parameters for the time-compression technique. Example 3—(a) LDF (600 MHz). Example 4—(b) LDF (1200 MHz).

we take some symmetric time interval, say $\pm\Delta T_d$, about the center of the time-compressed pulse, and we record the maximum and minimum pulse magnitudes, denoted by z_{max} and z_{min}, respectively. The *p-p* ripple distortion (over $\pm\Delta T_d$) is defined by

$$\text{RD} \triangleq 20 \log \left[\frac{z_{max} - z_{min}}{(z_{max} + z_{min})/2} \right], \tag{49}$$

where RD is in dB. Both z_{max} and z_{min} are positive because $A(t)$ is a positive pulse. We plot the *p-p* ripple distortion versus ΔT_d in Fig. 8. The largest ΔT_d is 16 μs because that is the edge of the compressed pulse. Although it is difficult to translate the meaning of RD to a TV quality measure, it can be certain that a large RD (i.e., large ripple) would mean poor transmission quality. To make a TV system workable, an RD of less than −45 dB is probably necessary, although other applications may not require such a low distortion.

Referring to Fig. 8, it is obvious that the distortion gets progressively smaller from examples 1 to 4. But the lowest distortions, despite the large BTs involved, are still too excessive for high quality TV transmission. Some more examples are provided in Appendix B for additional insight into the problem of ripple distortion.

3.3 An example of time compression and expansion

In this example, we use practical design parameters involving both time compression and time expansion (Fig. 9). Figure 9a shows a 64-

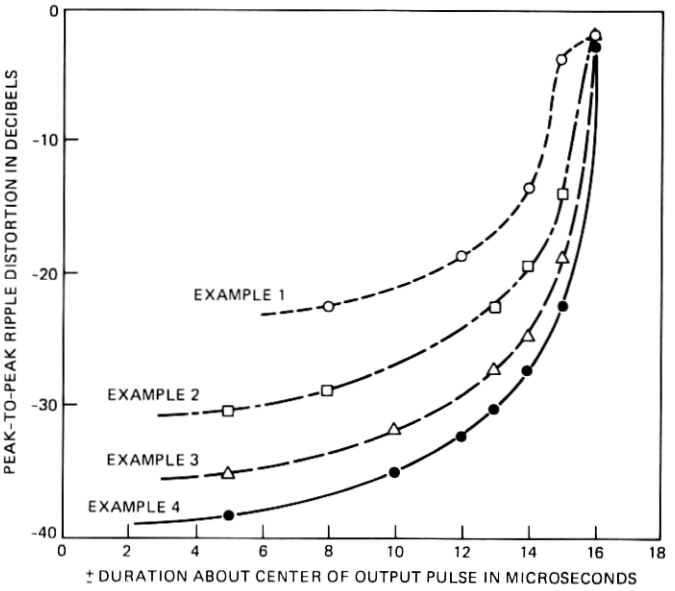

Fig. 8—Distortion results for time-compression examples.

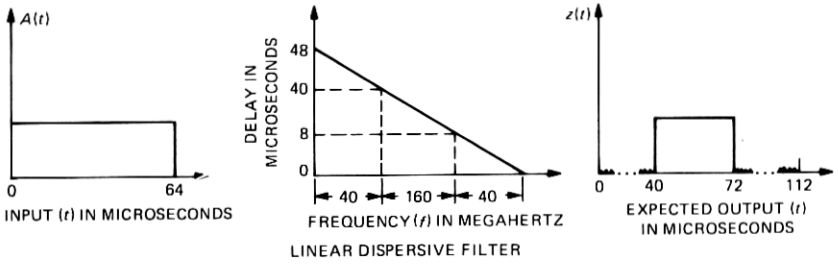

(a)

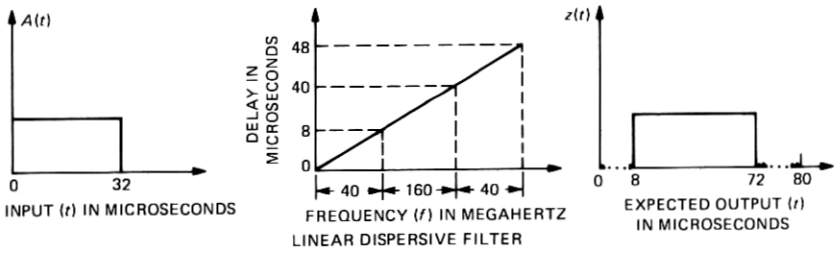

(b)

Fig. 9—Parameters for (a) time-compression and (b) time-expansion examples.

μs pulse as an input to the compressor, and the expected output. The actual ripple distortion (i.e., simulated result) over the 32-μs compressed pulse is shown in Fig. 10a. To check the operation of the expander alone, we assume an input of a 32-μs pulse to the expander. The expected result is shown in Fig. 9b, and the simulated ripple distortion is plotted in Fig. 10b. It is clear from Figs. 10a and 10b that both the compressor and the expander lead to considerable distortion.

To simulate a total system with compression and expansion, we used the distorted 32-μs pulse from the compressor as an input to the expander. The expanded output pulse is so distorted that it becomes meaningless to make a ripple distortion plot as before. Instead, we plot a small segment near the center of the expanded pulse in Fig. 10c to illustrate its excessive distortion. The performance of this total system is definitely not suitable for TV transmission. Some filterings were tried at the output of the expander, but little improvement was obtained.

IV. CONCLUSION

We have studied a time-compression technique based on a simple configuration of SAW filters. The technique was derived heuristically and can be viewed as a quasi-stationary model for the chirp signals. Numerical results show that excessive distortion is created, and its

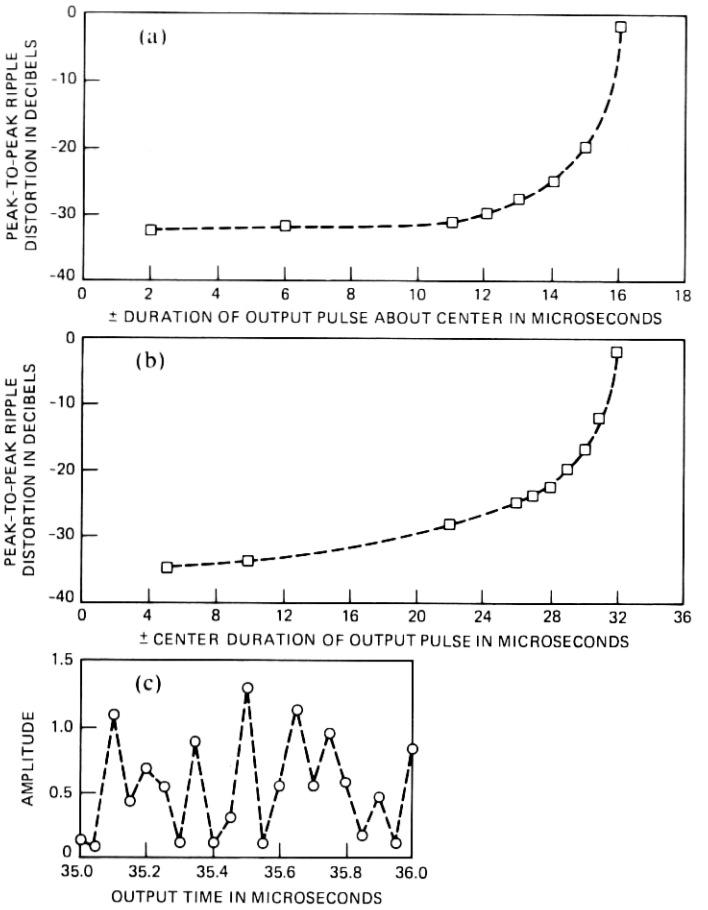

Fig. 10—Results for time-compression and time-expansion examples. (a) Ripple distortion of time-compression example. (b) Ripple distortion of time-expansion example. (c) Pulse ripple for time-compression and time-expansion examples.

application to TV transmission is not suitable unless some kind of equalization is provided. One such equalization is the chirp transform processor[3] which involves considerably more complexity. Simpler equalizations may be possible but do not seem to be straightforward. As for other applications where the distortion requirement is less stringent, this approach may be feasible.

V. ACKNOWLEDGMENTS

The authors wish to thank O.-C. Yue and L. A. Coldren for many helpful discussions. Some interesting discussions with T. Meeker at the early part of the study are also gratefully acknowledged.

APPENDIX A

Impulse Response of a Linear Dispersive Filter

A linear dispersive filter (LDF) is a filter having a linear delay characteristic. Using the analytic-signal notation, its transfer function can be written as

$$G(\omega) = \begin{cases} 1, & -\frac{\Delta\omega}{2} \le \omega - \omega_0 \le \frac{\Delta\omega}{2}, \\ 0, & \text{elsewhere} \end{cases} \tag{50}$$

and

$$D(\omega) = (\tau_0 - s\omega_0) + s\omega, \qquad -\frac{\Delta\omega}{2} \le \omega - \omega_0 \le \frac{\Delta\omega}{2}, \tag{51}$$

where $G(\omega)$ and $D(\omega)$ are the gain and group delay, respectively; ω_0 is the angular center frequency, and $\Delta\omega$ is the bandwidth in radians; τ_0 is the delay at ω_0; and $\Delta\tau$ is the delay dispersion over $\omega_0 + \Delta\omega/2$. The delay slope is defined by

$$s \triangleq \frac{\Delta\tau}{\Delta\omega}. \tag{52}$$

Integrating $D(\omega)$ with respect to ω, we obtain the phase,

$$\phi(\omega) = -(\tau_0 - s\omega_0)\omega - \frac{s}{2}\omega^2, \qquad -\frac{\Delta\omega}{2} \le \omega - \omega_0 \le \frac{\Delta\omega}{2}, \tag{53}$$

where the integration constant has been dropped for convenience. Using exponential notation and neglecting all unimportant multiplying constants and constant phase shifts in subsequent discussions, the impulse response of the LDF is

$$h(t) = \text{Re} \int_{\omega_0 - \frac{\Delta\omega}{2}}^{\omega_0 + \frac{\Delta\omega}{2}} \exp\left\{-j\left[(\tau_0 - s\omega_0)\omega + \frac{s}{2}\omega^2\right]\right\} \exp(j\omega t) d\omega. \tag{54}$$

The above is simply an inverse Fourier transform of the transfer function. By a change of variable, it can be rewritten as

$$h(t) = \text{Re} \exp(j\omega_0 t) \int_{-\frac{\Delta\omega}{2}}^{\frac{\Delta\omega}{2}} \exp\left[-j\left(\tau_0\omega + \frac{s}{2}\omega^2\right)\right] \exp(j\omega t) d\omega. \tag{55}$$

There are two methods to solve for $h(t)$ according to the above: (*i*) extend the limits of integration to $\pm\infty$ and obtain a closed form solution easily; (*ii*) retain the finite integration limits and derive the result using Fresnel integrals. Both methods are shown briefly below.

Method I

Changing the limits of integration to $\pm\infty$ in eq. (55) and recognizing that the integration of the term $\exp(-j\tau_o\omega)$ leads to a delay of τ_0 in $h(t)$, we obtain an integral in the form of

$$J = \int_{-\infty}^{\infty} \exp(-jk\omega^2)\exp(j\omega t)d\omega, \tag{56}$$

where k is a constant. Putting the integrand in Gaussian form by completing the square, we get

$$J = \sqrt{\frac{\pi}{k}} \exp\left[j\left(\frac{t^2}{4k} - \frac{\pi}{4}\right)\right]. \tag{57}$$

Applying the above to eq. (55), we obtain the desired result

$$h(t) = \text{Re } \exp(j\omega_0 t)\exp\left[j\frac{(t-\tau_0)^2}{2s}\right], \tag{58}$$

or

$$h(t) = \cos\left[\omega_0 t + \frac{(t-\tau_0)^2}{2s}\right]. \tag{59}$$

However, because the original transfer function has a delay dispersion $\Delta\tau$ defined about τ_0, the valid range of t for eq. (59) is

$$\tau_0 - \frac{\Delta\tau}{2} \le t \le \tau_0 + \frac{\Delta\tau}{2}. \tag{60}$$

Method II

Setting $\omega_1 = \omega_0 - \Delta\omega/2$ and $\tau_1 = \tau_0 - \Delta\tau/2$, eq. (55) is written as

$$h(t) = \text{Re } \exp(j\omega_1 t)\int_0^{\Delta\omega} \exp\left[-j\left(\tau_1\omega + \frac{s}{2}\omega^2\right)\right]\exp(j\omega t)d\omega. \tag{61}$$

Again recognizing that $\exp(-j\tau_1\omega)$ leads to a delay of τ_1, we may substitute $\tau = t - \tau_1$ and

$$h(\tau) = \text{Re } \exp(j\omega_1\tau)\int_0^{\Delta\omega} \exp\left(-j\frac{s}{2}\omega^2\right)\exp(j\omega t)d\omega. \tag{62}$$

Completing the square in the integrand, we obtain

$$h(\tau) = \text{Re } \exp(j\omega_1\tau)\exp\left(j\frac{\tau^2}{2s}\right)\int_0^{\Delta\omega} \exp\left[-j\frac{s}{2}\left(\omega - \frac{\tau}{2}\right)^2\right]d\omega. \tag{63}$$

The above can be integrated using Fresnel integrals, and the result is

$$h(\tau) = \text{Re} \exp\left[j\left(\omega_1\tau + \frac{\tau^2}{2s}\right)\right] \times\{[C(y_2) - C(y_1)] - j[S(y_2) - S(y_1)]\}, \quad (64)$$

where

$$y_1 \triangleq \sqrt{\frac{s}{\pi}}\Delta\omega\left(-\frac{\tau}{\Delta\tau}\right), \quad (65)$$

$$y_2 \triangleq \sqrt{\frac{s}{\pi}}\Delta\omega\left(1 - \frac{\tau}{\Delta\tau}\right). \quad (66)$$

$C(z)$ and $S(z)$ are the Fresnel integrals defined in eqs. (44) and (45). Consider the bracketed term:

$$[C(y_2) - C(y_1)] - j[S(y_2) - S(y_1)] \triangleq \rho(\tau)\exp[j\theta(\tau)]. \quad (67)$$

Neglecting small ripples, $\rho(\tau)$ is constant over $0 \le \tau \le \Delta\tau$ and vanishes outside this range. The phase term $\theta(\tau)$ is approximately constant over the same interval $0 \le \tau \le \Delta\tau$. Therefore, putting back the τ_1 delay, we have

$$h(t) \approx \text{Re} \exp\left\{j\left[\omega_1(t - \tau_1) + \frac{(t - \tau_1)^2}{2s}\right]\right\}. \quad (68)$$

APPENDIX B

Additional Examples On Ripple Distortion

Additional examples are provided here for more insight into the phenomenon of ripple distortion. The first case of interest is that of band-limiting effect on the input pulse. We use a 32-μs input pulse and low-pass filter it with a raised-cosine characteristic, where the gain is unity from zero to 8 MHz, 0.5 at 9 MHz, zero at 10 MHz, and the delay is constant over the passband. The output is, of course, a 32-μs pulse with ripples. The magnitude of these ripples are plotted in Fig. 11 in the manner similar to Figure 8.

The second case of interest is that of ripple distortion caused by the linear delay slope of the LDF. Three specific examples are provided to illustrate this effect:

Case A: The input to the time-compression filter is a 32-μs pulse. It is modulated by a CW frequency of $f_0 = 1600$ MHz. The LDF has a delay characteristic as shown in Fig. 1, where $f_0 = 1600$ MHz and $\Delta f = 2400$ MHz.

Case B: The conditions are identical to those of Case A, except $f_0 = 1000$ MHz and $\Delta f = 1200$ MHz.

Case C: The conditions are identical to those of Case A, except $f_0 = 700$ MHz and $\Delta f = 600$ MHz.

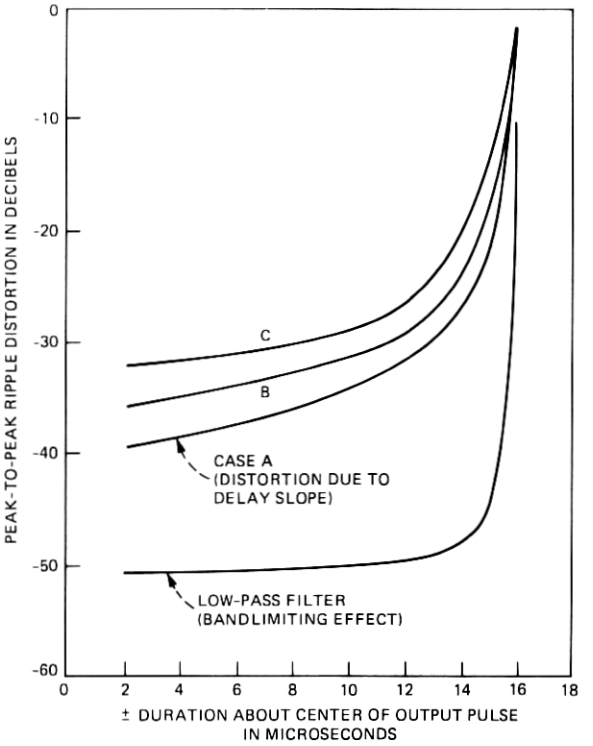

Fig. 11—Distortions because of bandlimiting and delay slope.

All three examples above illustrate the case of no time compression, but simply a constant delay through the LDF as viewed by the quasi-stationary model. Note that the magnitude of the delay slope increases by a factor of two from each example to the next and, hence, an increase in ripple distortion as seen from the results plotted in Fig. 11.

REFERENCES

1. J. E. Flood and D. I. Urguhart-Puller, "Time-Compression-Multiplex Transmission," Proc. IEE, *III,* No. 4 (April 1964), pp. 647–68.
2. D. H. Morgen and E. N. Protonotaries, "Time Compression Multiplexing For Loop Transmission of Speech Signals," IEEE Trans. Commun., *COM-22,* No. 12 (December 1974), pp. 1932–9.
3. Kai Y. Eng and On-Ching Yue, unpublished work.
4. J. R. Klauder et al., "The Theory and Design of Chirp Radars," B.S.T.J., *39,* No. 4 (July 1960), pp. 745–808.
5. M. A. Jack et al., "The Theory, Design, and Applications of Surface Acoustic Wave Fourier-Transform Processors," Proc. IEEE, *68,* No. 4 (April, 1980), pp. 450–68.